JOURNAL OF ELECTROMAGNETIC ENGINEERING AND SCIENCE, VOL. 23, NO. 2, 122~128, MAR. 2023

https://doi.org/10.26866/jees.2023.2.r.160
ISSN 2671-7263 (Online) · ISSN 2671-7255 (Print)

Experiments of Sub-THz Wave Folded Waveguide Traveling-Wave Tube Amplifier

Kwang-Ho Jang[1,2] · Jong-Hyun Kim[3] · Geun-Ju Kim[1] · Jung-Il Kim[1] · Jin-Joo Choi[2,*]

Abstract

This study showed the possibility of using a sub-terahertz (THz) traveling-wave tube (TWT) via measuring the transmission characteristics and TWT performance of the circuit by applying X-ray LIGA, a micro-fabrication process, to the interaction circuit. The applied circuit type, an E-bend folded waveguide, is a simple structure most suitable for lithography. A total of three applied frequencies were used the W-band, G-band, and 850 GHz. Among the manufactured circuits, the W-band circuit was applied to the TWT, one of the vacuum electronics devices (VEDs). This was done to prove the manufacturing accuracy of the circuit by comparing the nonlinear characteristics of the circuit with the prediction results. Through such testing, the small signal gain was measured as 13 ± 2 dB under the conditions of 13.96-kV and 24.2-mA electron beam energy. The frequency bandwidth was extremely wide, about 9 GHz, and showed similar characteristics to the simulation predictions. The maximum output of the device was obtained up to 1 W or more at 87.12 GHz by slightly increasing the beam current. These characteristic achievements showed the suitability of the TWT for very small circuits fabricated using the X-ray LIGA process, further suggesting the applicability of other sub-THz bands.

Key Words: Folded Waveguide, Micro-Fabrication, Sub-THz, TWT, X-Ray LIGA.

I. Introduction

In a vacuum tube such as a traveling-wave tube (TWT), extended interaction oscillator (EIO), and extended interaction klystron (EIK) that uses a linear beam, the size of the circuit becomes very small as the frequency increases [1]. Interaction circuits above sub-terahertz (THz) have a μm-unit circuit size; thus, there is a limit to such general machining. Therefore, micro-fabrication processes such as X-ray/UV lithography, electroplating, and polymer replication (LIGA), deep reactive ion etching (DRIE), nano-computer numerical control (CNC), 3D printing, and wire-electrical discharge machining (EDM) have been used to fabricate circuits [2]. Of these, we fabricated circuits using the X-ray LIGA process with good verticality because it has a simple structure in the form of a folded waveguide. We sought to check the applicability of sub-THz bands by making circuits not only in the W-band but also in the G-band and 850-GHz frequency band.

In this paper, circuits of various sub-THz frequencies were fabricated using the X-ray LIGA process and cold-tested to analyze transmission characteristics. Among them, the W-band circuit was composed of TWT designed to interact with the linear electron beam; the operation's functioning an amplifier was verified by performing a hot test.

Manuscript received August 31, 2022 ; Revised February 16, 2023 ; Accepted March 31, 2023. (ID No. 20220831-118J)
[1]Applied Electromagnetic Wave Research Center, Korea Electrotechnology Research Institute, Ansan, Korea.
[2]Department of Electronic Convergence Engineering, Kwangwoon University, Seoul, Korea.
[3]Industry Technology Convergence Center, Pohang Accelerator Laboratory, Pohang, Korea.
[*]Corresponding Author: Jin-Joo Choi (e-mail: jinchoi@kw.ac.kr)

II. DESIGN

The interaction circuit for the sub-THz TWT applied a folded waveguide structure, which is the simplest structure that can be easily used for X-ray LIGA processing. In this circuit, the rectangular waveguide is periodically structured as an E-bend and operates in the lowest TE_{01} mode. This circuit structurally delays the electromagnetic wave so that it interacts with the electron beam. It shows amplification characteristics by energy conversion in the synchronization of the phase velocity between the electron beam and the electromagnetic wave. This circuit has broadband characteristics and is synchronized over a relatively wide frequency range [3]. The basic structure was designed using the folded waveguide dispersion relationship and beam equation [4]. The length and structure of the circuit were designed by analyzing the nonlinear characteristics using the particle-in-cell (PIC) simulation code, considering the gains. The circuits were optimized as a two-stage structure with a total of 78 periods. In this circuit, the first stage has 29 periods, and the second stage has 49 periods. This is a structure that allows for stable operation without oscillation even when the gain is further increased [5]. The design parameters of circuits optimized with this structure are shown in Fig. 1. The W-band circuit is small at several hundred micrometers (μm), but in the case of 850 GHz, it is a very challenging value because it is small to 30 μm.

The designed circuit was manufactured by applying the X-ray LIGA process with a high aspect ratio and high accuracy, as general machining is less accurate than micro-fabrication [6, 7]. The X-ray LIGA for circuit fabrication proceeds through a four-step process. First, the positive photoresist (PR) applied to the copper base was exposed to X-rays through a gold-plated patterned X-ray mask. Second, the area around the exposed PR pattern was etched with a developer. Next, the existing copper is filled with copper plating around the patterned PR. Fig. 2 shows the circuits of the sub-THz band manufactured using this micro-fabrication process. As shown in this figure, not only can patterns with 270-μm spacing in the W-band circuit be manufactured without issues, but the same is true of very small patterns, with up to 30-μm spacing, in the 850-GHz band circuit. These circuits

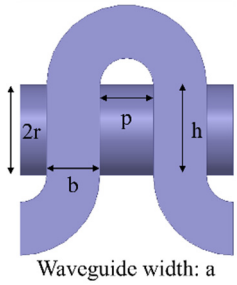

Dimension of Folded waveguide circuits

Unit: μm	W-band	G-band	850-GHz
a	1950	820	212
b	270	120	30
p	540	240	60
h	460	200	51
r	230	100	25

Fig. 1. Design result of the final optimized sub-THz folded waveguide circuit.

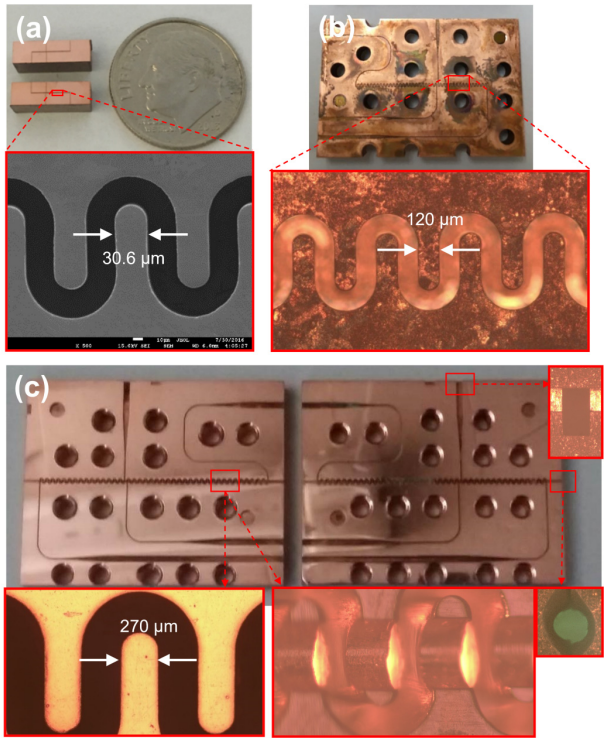

Fig. 2. Folded waveguide circuits manufactured using the X-ray LIGA process: (a) 850-GHz circuit, (b) G-band circuit, and (c) W-band circuit.

are patterned extremely precisely, and the tolerance for part of the circuit is ±1 μm [8].

Beam-tunnel processing was not included in the sub-THz circuit manufactured using the X-ray LIGA process. Because X-ray LIGA is a method of etching after exposure, only vertical pattern processing is possible. Therefore, the W-band circuit used to compose the TWT was processed by applying beam tunnel processing as an additional profile CNC process. This beam tunnel processing is applicable up to an 850-GHz circuit. Fig. 2(c) shows the completed W-band circuit. As shown in this figure, the folded waveguide pattern designed using the X-ray LIGA process was accurately produced, and the beam tunnel was also well machined. The processed circuit was aligned using the alignment pins so that the beam tunnel and input/output waveguide were positioned normally. In addition, we tried to verify the performance of these circuits by measuring the transmission characteristics and conducting electron-beam experiments.

First, the frequency transmission characteristics of the fabricated circuit were measured using a vector network analyzer (VNA) to measure the similarity with the designed circuit. Among the circuits, only the transmission characteristics of the W-band and G-band were measured using a VNA. Because it is extremely difficult to configure a measurement system to measure 850-GHz circuits, there was a limit to measuring all circuits. The fabricated 850-GHz circuit is meaningful in that it was

shown to make it possible to manufacture a very small structure highly accurately.

The transmission characteristics of the W-band and G-band circuits were measured with a two-port system as shown in Fig. 3(a) and 3(b). First, the W-band circuit was measured with a WR-10 waveguide extension (Anritsu, 3743A) using a VNA (Anritsu, MS4647B). The loss of the circuit calculated from the measured data was 0.42 dB/cm. The G-band circuit was measured with WR-3 (OML, V05VNA2-T/R-A) and WR-5 (OML, V03VNA2-T/R-A) waveguide extensions using PNA (Agilent, N5242A). The loss of the circuit calculated from the measured data was 1.57 dB/cm. As shown in Fig. 3(c) and 3(d), the measured transmission characteristics of the circuit were similar to the frequency bandwidth predicted by simulator (High Frequency Structure Simulator; Ansys Inc., Canonsburg, PA, USA). However, there was a slight difference between the simulation and measurement of the transmission characteristics. There are two main reasons for this the first is the decrease in conductivity due to the surface roughness of the circuits, and the second is the problem of misalignment in the arrangement of the measurement ports. These problems were verified by electromagnetic wave simulation [8].

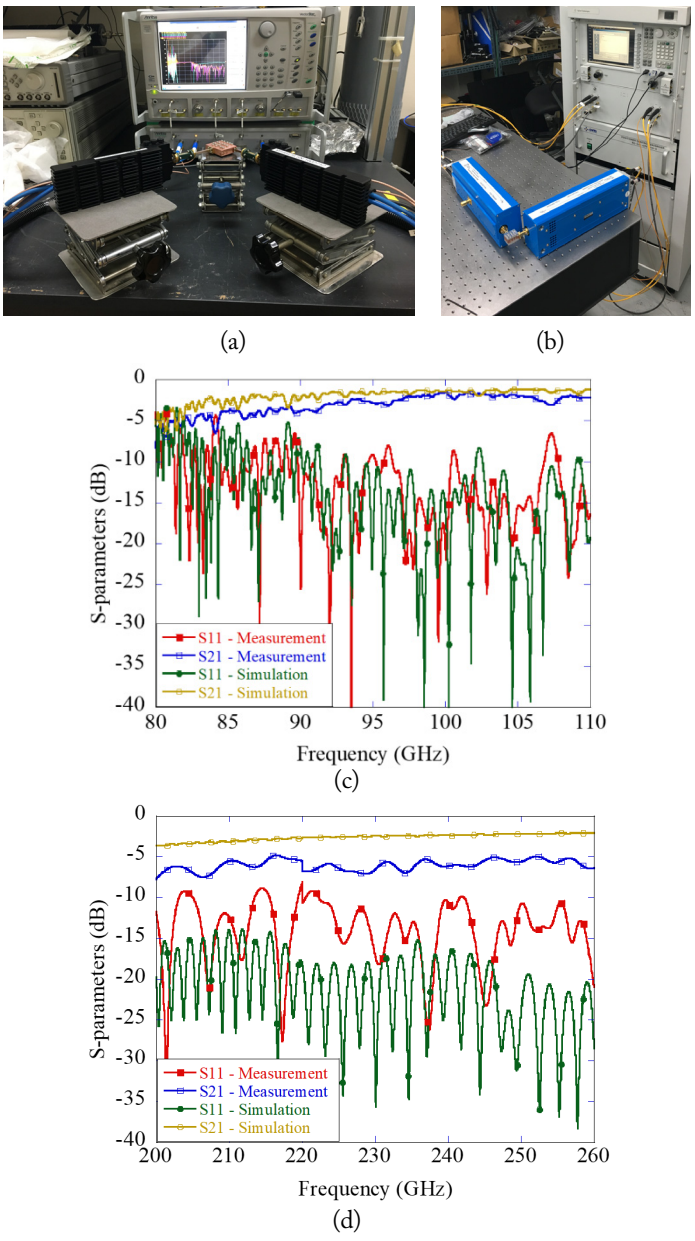

Fig. 3. Experimental configuration and results for measuring the transmission characteristics of fabricated circuits. Circuit measurement setup of (a) W-band and (b) G-band. Measurement and simulation data comparison graph of (c) W-band and (d) G-band.

III. Experiment

The measurement of the frequency characteristics of the fabricated sub-THz circuits has limitations in terms of its producing a practically accurate characteristic analysis. Therefore, it is necessary to check the output characteristics using the interactions between the electron beams and radiofrequency (RF). The circuit characteristics can be predicted through comparison using simulation. Among the fabricated sub-THz circuits, the folded waveguide TWT was constructed by applying the W-band circuit.

We prepared the simplest experimental configuration to verify the circuit performance as an amplifier. Fig. 4 shows the overall configuration of the W-band TWT. The applied parts of the TWT were as follows. The diode-type pierce gun for linear beams was assembled by hand in the laboratory using a bolt-and-nut combination method without brazing. The cathode and heater assembly used included an M-type cathode from HeatWave Labs Inc. The emission area was 2.54 mm^2, and the current density was 2 A/cm^2. A solenoidal magnet was used for the magnetic field circuit to control the electron beam. The electromagnet focused the magnetic field with a pole-piece and changed the current of three coils to obtain a flat magnetic field.

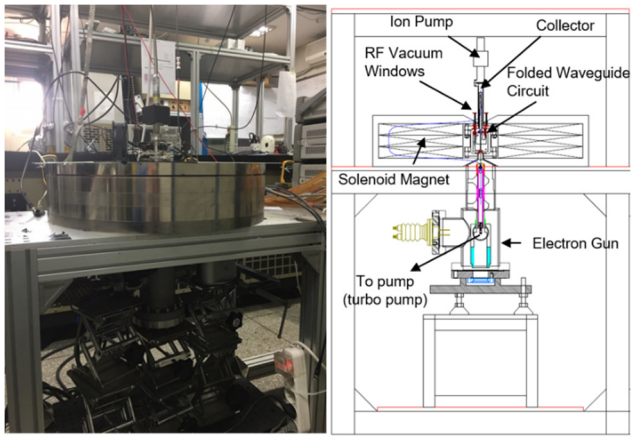

Fig. 4. Manufactured configuration and cross-sectional design view of the W-band traveling-wave tube.

In this case, the flat magnetic field was 4.8 kG, and the total length was about 60 mm. The installed vacuum window was not a typical pillbox type but the mica vacuum window in which a very thin dielectric is inserted. It is the simplest structure that can be operated by pulse operation. The window had a very wide broadband characteristic of about 40 GHz with return loss under −10 dB. The collector was made of oxygen-free high-conductivity copper (OFHC) in the form of a simple cylinder. It was designed to naturally spread the electron beam by reducing the magnetic field at the end of the circuit. The collision electron beam was designed so that the maximum unit area does not exceed 0.5 kW/cm^2. Furthermore, 2 L/s and 200 L/s pumps were configured on the collector side and the electron gun side, respectively, to maintain high vacuum. The tube was free-standing within the electromagnet bore. It may be necessary to adjust the axis of the tubing to adjust the beam alignment. These tube components were baked out between 100°C and 150°C before final assembly with the electromagnet. This was sufficient processing for the pulse experiment.

First, before operating the TWT, an electron beam emission test was conducted to verify the performance of the electron gun. The characteristics of the electron beam were measured and analyzed in two ways. One method entailed measuring the amount of current with the induced current of the cathode line, and the other method was to image and check the size and intensity. The amount of current was easily measured by connecting a current transformer (CT)-type Pearson coil to an oscilloscope. The electron beam was visualized by combining a 2.7-inch flanged viewport and a phosphor screen coated with ZnS(Ag) at the collector position.

The electromagnet for focusing the electron beam applied 96 A to each coil to create a flat magnetic field of 4.8 kG. The electron gun was operated with a short pulse of high voltage using a modulator (ETM, HVP4081), and the emission test was conducted while gradually increasing the voltage. The electron beam emission test result is shown in Fig. 5, indicating the amount of emitted electron beam current according to the voltage applied to the electron gun. The emission current of the electron gun was predicted according to the Child–Langmuir equation by the space-charge operation:

$$I = PV^{3/2}, \tag{1}$$

where P is the perveance of the electron gun. The perveance calculated by the E-gun simulation was 0.0256 μP under normal operating conditions. The calculated perveance predicted the emission current, showing similar characteristics to the measured emission current as depicted in the graph. The results of the test confirmed that the electron beam was emitted up to 57 mA under the condition of a maximum voltage of −17 kV. The emitted and focused electron beam passes

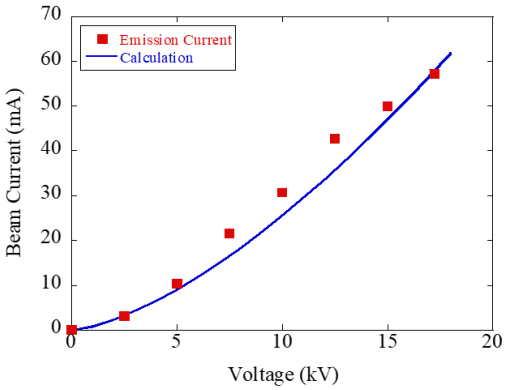

Fig. 5. Electron beam test results of the electron gun installed with the traveling-wave tube. The red dots represent the emission currents obtained through the experiment, and the blue line is the predicted value calculated by perveance.

through the beam tunnel and finally hits the phosphor screen to emit blue light. The intensity of the brightness depends on the energy level of the electron beam. Changes appearing on the phosphor screen make it possible to roughly predict electron beam intensity, size, and alignment. Fig. 6 shows the visualized characteristic difference between the high-energy electron beam and the low-energy electron beam. The size and alignment of the electron beam could be roughly predicted, but it was important that the actual circuit was positioned accurately. Therefore, the alignment and control of the electron beam was performed after precise circuit arrangement.

The configured TWT was prepared for a hot test experiment to verify the amplification performance of the electromagnetic waves by emitting electron beams. Fig. 7 shows the practical experimental setup. In this system, a high voltage was applied to the cathode using an ETM modulator to emit the electron beam, and a high current was applied to a coil using a high-current power supply to focus the electron beam. The input power for the TWT was provided by solid-state amplifier modules. The input source of the amplifier multiplier chain (AMC) from Millisys (Gwangju, Korea) provided up to 20 dBm of power from 85 to 96 GHz. The output power of the

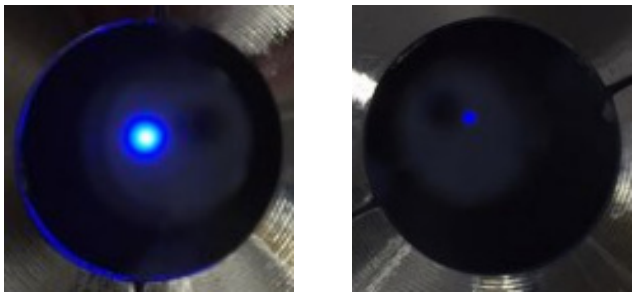

(a) (b)

Fig. 6. Phosphor screen electron beam collision imaging as dependent on energy intensity: (a) high-energy beam and (b) low-energy beam.

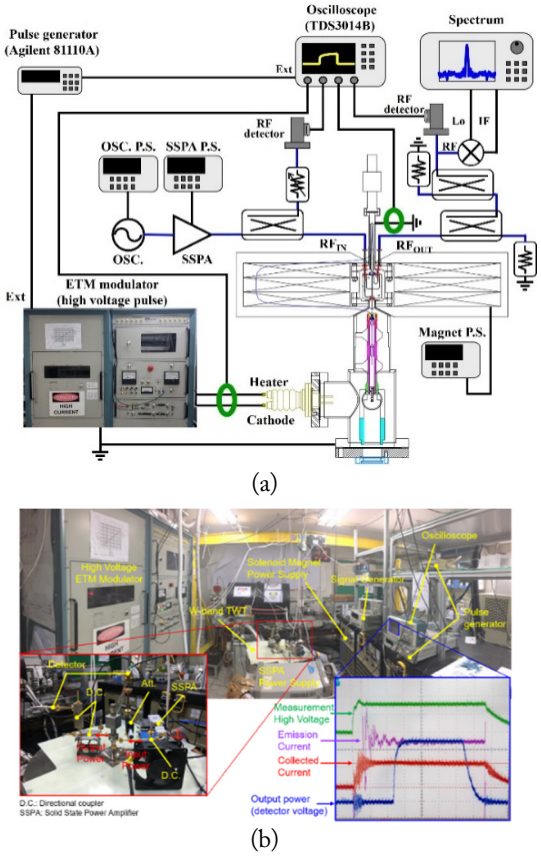

Fig. 7. Configuration of hot-test experiment for traveling-wave tube performance verification: (a) block diagram and (b) test set-up.

input source differs depending on the frequency change, so the directional coupler was connected to monitor the input power to the TWT in real time. The output signal of the TWT was branched to a directional coupler and measured by a Schottky diode–type detector. The electron beam transmission efficiency was obtained by calculating the emission current and collection current measured by the Pearson coil. The TWT was tested using two pulse timings to clearly observe its operation as an amplifier. Therefore, high-voltage timing and RF timing applied differently. This made it easy to distinguish RF amplification and oscillation phenomena in the TWT hot test.

After the electron beam test, the TWT circuit was installed in the tubing and assembled with an electromagnet. In order to optimize the alignment, the assembly tolerance of each part was brought to within 10 μm while assembling the electron gun directly in the lab. The anode was placed at the tip of the electron gun, which was directly connected to the circuit through physical alignment. Before that, the circuit was aligned to the center of the tubing, and we sought to have an error of about 10 μm. Significant effort was put into alignment during the installation process, but the maximum electron beam transmission efficiency was possible up to about 50%. Indeed, it is not easy to precisely pass an electron beam about the thickness of a hair through a circuit. This transmission problem may be due to very slight misalignment between the electron beam and the circuitry. A hot test was conducted to verify the performance of the TWT under this electron beam condition, and the results are shown in Figs. 8 and 9. The gain at saturated power had a characteristic degradation due to the small electron beam current. Therefore, we tried to confirm the amplification performance and broadband characteristics of the circuit by analyzing the small signal gain. In this condition, the operating voltage was −13.96 kV, and the beam current was 24 mA. As shown in Fig. 8(a), when a low input signal, represented by the blue line, was applied, the small signal gain was about 13±2 dB, as depicted by the red line. The TWT input power showed non-flat power characteristics due to the characteristics of the drive amplifier. For this reason, it is difficult to represent the exact frequency bandwidth of the gain.

Therefore, we must refer to the bandwidth for the saturated output power in Fig. 8(b). In this condition, the bandwidth was shown to be about 9 GHz, also showing similar characteristics to the simulation results at the lowered electron beam current of 24 mA. In the simulation (CTS Studio Suite - Charged Particle

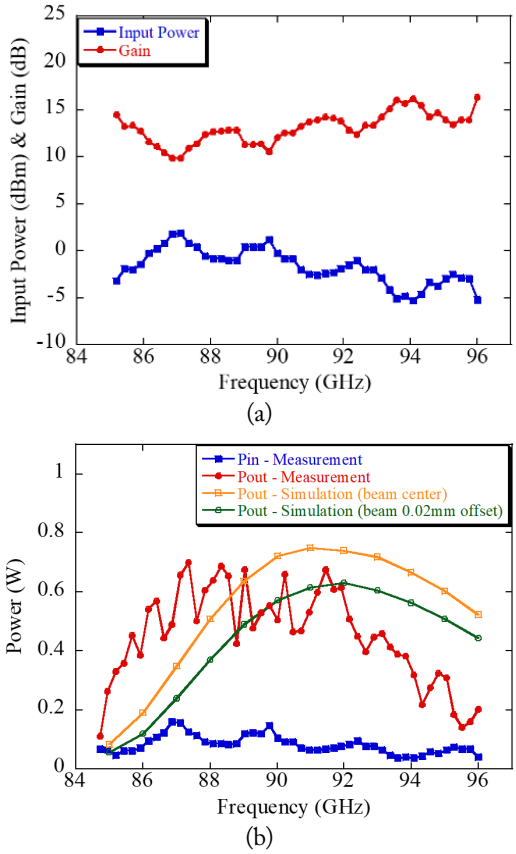

Fig. 8. Frequency versus power results of traveling-wave tube experiment when beam voltage was −13.96 kV and the collected electron beam current was 24.2 mA in the hot test: (a) small signal gain and (b) measurement results and simulation comparison results.

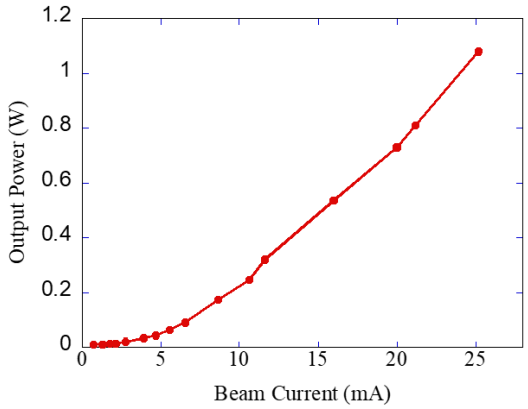

Fig. 9. Results of output power versus increasing collected current. The measurement frequency was 87.12 GHz, and the beam voltage was −14.14 kV.

Simulation; Dassault Systèmes, Paris, France), the input power was fixed at 20 dBm. The orange line indicates the condition that the electron beam is in the center, and the green line is the output characteristic of the offset electron beam. Compared with this result, when analyzed, the measured result showed that the electron beam was offset, while the transmission efficiency decreased. Here, the performance at high frequencies varied, but this was due to performance degradation at high frequencies of the drive power. Similarly, the low frequency measurement output was due to the slightly higher input power. These similar characteristics confirmed the amplification performance as well as the transmission characteristics according to the precision processing of the W-band circuit.

Additionally, the limited output power of the circuit could be increased by increasing the beam current. Such evidence shows that with increasing beam current, the circuit output power increased without saturation, as shown in Fig. 9. Since the electron beam transmission current efficiency cannot be adjusted, the heater temperature was increased to obtain a larger collection current. As a result, when the collector current was 25.2 mA, it showed the device output power characteristics of 1 W or more. Furthermore, this showed that an output of several watts (W) or more is not problematic if sufficient electron beam current is supplied. Of course, this requires improvement of the electron beam stick alignment.

IV. Conclusion

The sub-THz circuits were successfully fabricated by applying X-ray LIGA, one of the micro-fabrication processes. This represents one way to more accurately process a smaller circuit size as the frequency increases. The applied interaction circuits were the W-band, G-band, and 850 GHz among sub-THz frequencies, and each was designed and precisely manufactured. In the 850-GHz frequency band, the transmission characteristics were not measured due to the absence of measurement equipment, but it showed a highly accurate processing error of about ±1 μm. Instead, the transmission characteristics of the W-band and G-band could be measured in full frequency using VNA. As a result of measuring the transmission characteristics among the manufactured circuits, the W-band and G-band showed circuit loss of 0.42 dB/cm and 1.57 dB/cm, respectively.

Among the manufactured circuits, the W-band circuit was applied to the TWT to verify the nonlinear operating characteristics as an interaction circuit. The simplest type of mica window was applied to the RF vacuum window, and the electron-beam focusing was controlled by an electromagnet. A linear beam–type pierce gun was applied to the W-band TWT, and operation performance up to 50 mA was verified. Although precise alignment was attempted for the TWT combining circuits, the electron beam test results showed that the electron beam transmission efficiency was a maximum of 50%. As a result of the hot test, the small signal gain showed a characteristic of 13 ± 2 dB under the electron beam of 24.2 mA. As well, the bandwidth was measured at about 9 GHz and showed characteristics similar to the output results predicted in the simulation. As a result of increasing the transmission electron beam by instantaneously increasing the temperature of the cathode heater, the output was measured up to 1 W, showing an increasing trend without saturation. This showed that greater power is also possible if the electron beam transmission efficiency is increased. The circuit processed by X-ray LIGA was successfully fabricated, and the TWT of the W-band was tested and compared with the simulation to show similar performance. This means that the circuit produced by the X-ray LIGA was produced considerably accurately, suggesting the possibility of extending the applied micro-fabrication process to other sub-THz frequencies.

The authors would like to acknowledge financial support from the Agency for Defense Development, Republic of Korea and United States Office of Naval Research (No. N00014-20-1-2056). This work was supported in part by Korea Electrotechnology Research Institute (KERI) Primary research program through the National Research Council of Science & Technology (NST) funded by the Ministry of Science and ICT (MSIT) (No. 23A01072).

References

[1] J. H. Booske, R. J. Dobbs, C. D. Joye, C. L. Kory, G. R. Neil, G. S. Park, J. Park, and R. J. Temkin, "Vacuum electronic high power terahertz sources," *IEEE Transactions on Terahertz Science and Technology*, vol. 1, no. 1, pp. 54-75, 2011.

[2] A. M. Cook, C. D. Joye, and J. P. Calame, "W-band and D-band traveling-wave tube circuits fabricated by 3D printing," *IEEE Access*, vol. 7, pp. 72561-72566, 2019.
[3] G. Dohler, D. Gagne, D. Gallagher, and R. Moats, "Serpentine waveguide TWT," in *Proceedings of 1987 International Electron Devices Meeting*, Washington, DC, 1987, pp. 485-488.
[4] Y. H. Na, S. W. Chung, J. J. Choi, "Analysis of a broadband Q band folded waveguide traveling-wave tube," *IEEE Transactions on Plasma Science*, vol. 30, no. 3, pp. 1017-1023, 2002.
[5] Z. Zhang, C. Ruan, A. K. Fahad, C. Zhang, Y. Su, P. Wang, and W. He, "Multiple-beam and double-mode staggered double vane travelling wave tube with ultra-wide band," *Scientific Reports*, vol. 10, no. 1, article no. 20159, 2020. https://doi.org/10.1038/s41598-020-77204-w
[6] Y. M. Shin, J. K. So, S. T. Han, K. H. Jang, G. S. Park, J. H. Kim, and S. S. Chang, "Microfabrication of millimeter wave vacuum electron devices by two-step deep-etch x-ray lithography," *Applied Physics Letters*, vol. 88, no. 9, article no. 091916, 2006. https://doi.org/10.1063/1.2178770
[7] A. L. Bogdanov and S. S. Peredkov, "Use of SU-8 photoresist for very high aspect ratio x-ray lithography," *Microelectronic Engineering*, vol. 53, no. 1-4, pp. 493-496, 2000.
[8] K. H. Jang, J. J. Choi, and J. H. Kim, "X-ray LIGA microfabricated circuits for a sub-THz wave folded waveguide traveling-wave-tube amplifier," *Journal of the Korean Physical Society*, vol. 75, pp. 716-723, 2019.

Kwang-ho Jang

received the B.S., M.S., and Ph.D. degrees in wireless communications engineering all from the Kwangwoon University, Seoul, Korea, in 2012, 2014, and 2018, respectively. From 2018 to 2021, he has been a postdoc-toral researcher with Korea Institute of Fusion Energy (KFE), Daejeon, Korea. Since 2021, he has been with the Korea Electrotechnology Research Institute, Ansan, Korea, where he is currently a senior researcher with the Applied Electromagnetic Wave Research Center. His research interests include high-power vacuum electronics and applications.

Jong-Hyun Kim

received his B.S. and M.S degrees in physics and electronic engineering from Kyungpook National University, Korea, in 2000 and 2002, respectively and his Ph.D. degree from Pohang University of Science and Technology (POSTECH) at Pohang, Korea, in 2014. From 2002 to 2003, he was a researcher at LG electronics Corporation. He joined Pohang Accelerator Laboratory (PAL) in 2003, where he is currently a senior scientist in Industry Technology Convergence Center, PAL and affiliate faculty in Department of Mechanical Engineering, POSTECH. His current research interests include micro-fabrication using X-ray lithography, X-ray based imaging for investigating material characterizations and other applications of synchrotron radiation.

Jung-Il Kim

received a Ph.D. from the School of Physics, Seoul National University (SNU), Seoul, Korea, in 2006. Since 2006, he has been with the KERI, Korea. His current position is principal researcher. His research interests include high-power vacuum electronic devices, from microwave to terahertz wave; terahertz imaging systems; medical linear accelerators (LINACs); and high-precision radiotherapy systems.

Geun-Ju Kim

received a Ph.D. in electrical and electronics engineering from the Korea Maritime & Ocean University (KMOU), Busan, Korea, in 2018. He joined the Korea Electrotechnology Research Institute, Korea, in 2004. He is currently working at the Applied Electromagnetic Wave Research Center of the Ansan Branch, Korea. His current position is principal researcher. His current research interests include THz imaging and applications, high-power electromagnetic wave devices and applications, and radiation therapy.

Jin-Joo Choi

received the B.S. degree in physics from Seoul National University, Seoul, Korea, in 1983, the M.S. degree in physics from Georgia State University, Atlanta, in 1985, and the Ph.D. degree in nuclear engineering from the University of Michigan, Ann Arbor, in 1991. In 1991, he was with the Vacuum Electronics Branch, Electronic Science and Technology Division, U.S. Naval Research Laboratory (NRL), Washington, DC. His work at the NRL was on the development of high-power millimeter-wave gyro amplifiers for electronic warfare and radar applications. Since 1997, he has been with the Kwangwoon University, Seoul, where he is currently a professor with the Department of Wireless Communications Engineering. His research interests include high-power vacuum electronics and passive and active solid-state devices.